Postprint of: Głowienka D., Szmytkowski J.: Influence of excitons interaction with charge carriers on photovoltaic parameters in organic solar cells. CHEMICAL PHYSICS. Vol. 503, (2018), p. 31 - 38. DOI: 10.1016/j.chemphys.2018.02.004

Influence of excitons interaction with charge carriers on photovoltaic parameters in organic solar cells

Damian Głowienka[1] and Jędrzej Szmytkowski[2]

Faculty of Applied Physics and Mathematics, Gdańsk University of Technology, Narutowicza 11/12, 80-233 Gdańsk, Poland

Abstract

We report on theoretical analysis of excitons annihilation on charge carriers in organic solar cells. Numerical calculations based on transient one–dimensional drift–diffusion model have been carried out. An impact of three quantities (an annihilation rate constant, an exciton mobility and a recombination reduction factor) on current density and concentrations of charge carriers and excitons is investigated. Finally, we discuss the influence of excitons interaction with electrons and holes on four photovoltaic parameters (a short–circuit current, an open–circuit voltage, a fill factor and a power conversion efficiency). The conclusion is that the annihilation

23 January 2018

process visibly decreases the efficiency of organic photocells, if the annihilation rate constant is greater than 10^{-15} m^3 s^{-1}.

Key words: Organic solar cells, Organic photovoltaics, Excitons

PACS: 71.35.-y, 73.50.-h, 73.50.Pz

1 Introduction

Currently, a great progress in the areas of molecular electronics and organic photovoltaics is observed. Nevertheless, devices based on inorganic materials are still more popular due to their better stability and efficiency. In order to obtain more efficient organic solar cells, it is important to solve a problem which physical processes significantly influence photovoltaic parameters, such as a short–circuit current (J_{sc}), an open–circuit voltage (V_{oc}), a fill factor (FF) and a power conversion efficiency (PCE). In contrast to inorganic photocells, the role of excitons is greater for organic structures [1,2]. For example, a photogeneration of charge carriers occurs as a consequence of excitons dissociation into separated electrons and holes. It seems that also other excitonic processes should give a visible contribution to photoelectric properties of such systems. Therefore, systematical studies of all excitonic effects are of great importance to obtain organic solar cells with higher efficiency.

One of the processes which can occur in molecular systems is the annihilation of excitons on charge carriers [3,4]. Considering a simple scheme of this phenomenon, an electron (a hole), which is a part of an exciton, interacts with

Email addresses: [1] dglowienka@mif.pg.gda.pl, [2] jedrek@mif.pg.gda.pl (Damian Głowienka[1] and Jędrzej Szmytkowski[2]).

a separated hole (electron). As a consequence, both interacting opposite sign charge carriers annihilate and a hole (an electron) from the interacting exciton becomes a free carrier. An alternative interpretation of this process takes into account a total energy transfer from an exciton to a separated charge carrier. As a result, the exciton is fully quenched. For both scenarios of this effect, a concentration of excitons decreases but concentrations of free electrons and holes are still the same. Recently, the annihilation of excitons on charge carriers has been intensively studied in organic light–emitting diodes [5–11], organic solar cells [12–20] and organic light–emitting transistors [21]. It is believed that this process should give a significant contribution to the loss of efficiency of these organic optoelectronic devices, especially for high excitation densities [15,22].

The aim of this paper is to investigate an influence of the excitons annihilation on photovoltaic parameters (J_{sc}, V_{oc}, FF and PCE) of organic solar cells under AM 1.5G irradiation which simulates a Sun light in laboratories. In order to achieve this goal, we decided to implement the annihilation process into the one–dimensional transient drift–diffusion model. As to our knowledge [23], the terms concerning the excitons annihilation on charge carriers have not been incorporated to time–dependent drift–diffusion equations by other researchers.

2 Model

First, it should be mentioned about several assumptions used in the presented model. Similarly to earlier numerical studies [24–30], we treat the recombination of charge carriers as a bimolecular process. For simplicity, thermionic and excitonic injection currents from electrodes are not taken into account. In

general, the intensity of light decreases exponentially due to absorption. This effect causes that most of light is absorbed near illuminated surface. Thus, it is convenient to assume that an illumination is uniform in the whole volume of a very thin sample what leads to a constant value of an exciton generation rate. In addition, we have decided to neglect the exciton–exciton interaction.

Excitons can interact with trapped and free (predominantly slow) charge carriers. Both these mechanisms are characterized by different rate constants. It has been experimentally demonstrated that an annihilation rate constant for the exciton–trapped charge carrier interaction can be even three orders of magnitudes lower than an annihilation rate constant which describes the exciton–free carrier interaction in the same material (anthracene) [31]. Therefore we decided to ignore trapping and detrapping effects in our calculations.

Continuity equations for excitons, electrons and holes are given by relations

$$\frac{\partial S}{\partial t} = G + \frac{1}{4}R_B - \frac{S}{\tau_s} - k_{diss}\left(E\right)S - \gamma_{ns}nS - \gamma_{ps}pS - \frac{1}{q}\frac{\partial J_s}{\partial x}, \tag{1}$$

$$\frac{\partial n}{\partial t} = k_{diss}\left(E\right)S - R_B + \frac{1}{q}\frac{\partial J_n}{\partial x} \tag{2}$$

and

$$\frac{\partial p}{\partial t} = k_{diss}\left(E\right)S - R_B - \frac{1}{q}\frac{\partial J_p}{\partial x}, \tag{3}$$

respectively, where S is a concentration of excitons, n and p are concentrations of electrons and holes, respectively, q is an elementary charge, G represents an exciton generation rate, τ_s is a lifetime of excitons, $k_{diss}\left(E\right)$ is an electric field dependent exciton dissociation rate, γ_{ns} and γ_{ps} are the second order rate constants for the annihilation of excitons on electrons and holes, respectively,

and R_B is a bimolecular recombination rate for electrons and holes. A term with a factor 1/4 in Eq. (1) is a consequence of an assumption that 25% of recombining electrons and holes form excitons [26]. It should be noted that terms with the rate constants γ_{ns} and γ_{ps} are not included in Eqs. (2) and (3) because the concentrations of free charge carriers do not change in the process of excitons annihilation.

Current densities of excitons (J_s), electrons (J_n) and holes (J_p) are given by

$$J_s = -\mu_s k_B T \frac{\partial S}{\partial x}, \tag{4}$$

$$J_n = -qn\mu_n \frac{\partial \phi}{\partial x} + \mu_n k_B T \frac{\partial n}{\partial x} \tag{5}$$

and

$$J_p = -qp\mu_p \frac{\partial \phi}{\partial x} - \mu_p k_B T \frac{\partial p}{\partial x}, \tag{6}$$

respectively, where μ_s is a mobility of excitons, μ_n and μ_p represent mobilities of electrons and holes, respectively, k_B is a Boltzmann constant and T is a temperature. Here, we have assumed a validity of the Einstein relation ($D_{n,p,s}/\mu_{n,p,s} = k_B T/q$, where D_j, with $j \in \{n, p, s\}$, is a diffusion coefficient for electrons, holes and excitons, respectively). Similarly to other authors [26,30,32,33], we have decided to use the exciton mobility instead of the exciton diffusion coefficient.

A local electric potential ϕ can be found from the Poisson equation

$$\frac{\partial^2 \phi}{\partial x^2} = -\frac{q}{\varepsilon_0 \varepsilon_r} (p - n), \tag{7}$$

where ε_0 is a vacuum permittivity and ε_r represents a dielectric constant

of material. Thus, an electric field can be calculated from the relation $E = -\partial\phi/\partial x$.

The bimolecular recombination rate R_B can be expressed as

$$R_B = \xi\gamma_L \left(np - n_{int}^2\right), \tag{8}$$

where ξ is a recombination reduction factor ($\xi \leq 1$), n_{int} represents the intrinsic carrier density in the bulk of material, and γ_L is a Langevin recombination coefficient, which is defined as

$$\gamma_L = \frac{q}{\varepsilon_0\varepsilon_r}\left(\mu_n + \mu_p\right). \tag{9}$$

In order to determine the rate $k_{diss}(E)$, we assume that the dissociation of excitons into separated electrons and holes is described by the Onsager–Braun formalism [34,35]. Thus, the overall exciton dissociation probability can be expressed as [24,36]

$$D\left(E\right) = \int_0^\infty P\left(E,a\right) F\left(a\right) da, \tag{10}$$

where the probability of dissociation P for an exciton separation distance a is given by

$$P\left(E,a\right) = \frac{k_{diss}\left(E\right)}{k_{diss}\left(E\right) + k_f} \tag{11}$$

and F represents a normalized distribution function which is defined as [24,36]

$$F\left(a\right) = \frac{4}{\sqrt{\pi}\, a_0^3}\, a^2 \exp\left(-\frac{a^2}{a_0^2}\right). \tag{12}$$

In the above equations k_f is a decay rate of excitons ($k_f = 1/\tau_s$) and a_0 is an initial exciton separation distance.

The exciton dissociation rate can be expressed as

$$k_{diss}\left(E\right)=\frac{3q}{4\pi\varepsilon_0\varepsilon_r a^3}\left(\mu_n+\mu_p\right)\exp\left(-\frac{r}{a}\right)\frac{J_1\left(2\sqrt{-2b}\right)}{\sqrt{-2b}}, \tag{13}$$

where J_1 is the first–order Bessel function, r is the Coulombic radius defined as

$$r=\frac{q^2}{4\pi\varepsilon_0\varepsilon_r k_B T} \tag{14}$$

and b is the electric field parameter given by

$$b=\frac{q^3 E}{8\pi\varepsilon_0\varepsilon_r k_B^2 T^2}. \tag{15}$$

Boundary conditions for electric potential are taken as

$$\phi(0)=V_{built}-V_a,\quad \phi(L)=0, \tag{16}$$

where V_{built} is a built–in voltage and V_a represents an applied voltage.

We assume that both electrodes form Schottky contacts. Therefore, the concentrations of electrons at both electrodes can be expressed as

$$n(0)=N_c\exp\left(\frac{-\phi_n}{k_B T}\right), \tag{17}$$

$$n(L)=N_c\exp\left(\frac{\phi_p-E_g}{k_B T}\right) \tag{18}$$

and boundary concentrations of holes are

$$p(0)=N_v\exp\left(\frac{\phi_n-E_g}{k_B T}\right), \tag{19}$$

$$p(L)=N_v\exp\left(\frac{-\phi_p}{k_B T}\right), \tag{20}$$

where L is a thickness of photoactive material, N_c and N_v are the effective densities of states in conduction and valence bands, respectively, ϕ_n and ϕ_p represent Schottky barrier heights for both electrodes and E_g is an energy band–gap.

If injection currents are neglected, then boundary conditions for the electron and hole current densities are

$$J_n(0) = 0, \quad J_n(L) = 0, \quad J_p(0) = 0, \quad J_p(L) = 0. \tag{21}$$

In the absence of excitonic injection from contacts, it is convenient to assume that concentrations of excitons at both electrodes are

$$S(0) = 0, \quad S(L) = 0. \tag{22}$$

Initial conditions (for $t = 0$) are assumed zero for all parameters.

The set of partial differential equations has been numerically solved with the Scharfetter–Gummel method. A detailed discretization procedure is presented in supplementary material. Our own numerical code was written in C++. A validity of the model has been proved by fitting of an experimental J–V characteristics (AM 1.5G illumination, room temperature) extracted from literature [37]. This fit is presented in Fig. 1. It should be noted that the exciton annihilation on charge carriers has not been considered here ($\gamma_{ns} = \gamma_{ps} = 0$) because such a process was not taken into account in the interpretation of these experimental results [37]. However, we were also able to achieve a satisfactory fit when these annihilation parameters were not equal to zero (not shown here). All parameters obtained from the fitting are listed in Table 1. If a reference is given in Table 1, it means that the parameter is fixed. The Schottky barrier

heights, an energy band–gap and a built–in voltage have been taken from an energy level diagram which is presented in supplementary material (Fig. S1). The mobilities of charge carriers were treated as free parameters in the fitting procedure. However, their final values are close to the magnitudes reported in literature [24,30,37,38].

We should also mention about an additional estimation used in our calculations. The electric field dependent exciton dissociation rate $k_{diss}(E)$ given by Eq. (13) has been chosen from the Onsager–Brown model [35] which is usually applied to simulate organic bulk heterojunction solar cells. However, it seems that this well–known model is only approximately valid. A more accurately formulated theory based on better physical conditions has been recently proposed by Hilczer and Tachiya [39]. They derived new analytical expressions for the exciton dissociation probability and the dissociation rate.

3 Results and discussion

This paragraph is organized as follows. First, we consider an influence of the annihilation rate constants on current densities and photovoltaic parameters. The next step is to analyze the impact of the exciton mobility μ_s on these quantities. Finally, the role of recombination reduction factor ξ is investigated. For all calculations, we decided to choose the same values of parameters which are listed in Table 1.

3.1 Influence of annihilation rate constant

The magnitudes of the rates γ_{ns} and γ_{ps} are in very wide ranges, usually between 10^{-18}–10^{-15} m^3 s^{-1}. Recently, it has been reported that the parameter γ_{ps} can achieve a value of 3×10^{-14} m^3 s^{-1} for the material which is often used in organic photovoltaics (P3HT) [12]. Therefore, a similar maximal values of the γ_{cs}, with $c \in \{n, p\}$, are used in our simulations. In this paper, the results obtained for $\gamma_{ns} = \gamma_{ps}$ will be presented. Thus, we shall often use a symbol γ_{cs} in notation. Fig. 2 shows an influence of the annihilation rate constant at short–circuit (SC) conditions. Part (a) illustrates the total current density versus voltage calculated for different γ_{cs}. For clarity, we have decided not to plot the results obtained for the annihilation rate constants lower than 10^{-15} m^3 s^{-1} because these J–V characteristics lie very close to the curve calculated for $\gamma_{cs} = 10^{-15}$ m^3 s^{-1} (see supplementary material, Fig. S2). It should be also mentioned that when the exciton annihilation is not taken into account ($\gamma_{cs} = 0$), then the J–V curve is identical to other J–V characteristics obtained for $\gamma_{cs} \approx 10^{-18}$–$10^{-17}$ m^3 s^{-1}. In Fig. 2(a), we observe that the current density reaches larger values of short–circuit current J_{sc} for lower magnitudes of the rate constants (J_{sc} is equal to an absolute value of a negative current density). It is clearly seen that the shapes of J–V characteristics significantly change. Obviously, this effect influences other photovoltaic parameters what will be demonstrated in further part of this paper. Fig. 2(b) presents spatial distributions of current components for electrons (J_n) and holes (J_p). Both distributions exhibit linear dependencies in the bulk of organic material. This result has been explained as a consequence of a large internal electric field at SC conditions [24,30]. Our simulations indicate that higher values of γ_{cs} cause

a monotonic decreasing of $|J_n|$ and $|J_p|$. Parts (c) and (d) of Fig. 2 demonstrate spatial distributions of charge carriers and excitons, respectively. Due to differences between the mobilities of electrons and holes, we observe that the hole density is around one order of magnitude larger than the density of electrons. The increasing of annihilation rate constant leads to a slight drop of the concentrations n and p. The density of excitons S also decreases for larger γ_{cs} due to higher probability of the annihilation process. It causes that less excitons can dissociate into separated charge carriers. Consequently, lower concentrations of electrons and holes are observed. We can see that different charge carrier mobilities lead to an asymmetrical shape of $S(x)$ curve. In our calculations $\mu_n > \mu_p$, therefore the probability of the excitons annihilation on charge carriers increases for slower holes. We should note that other calculations carried out for $\mu_n = \mu_p$ led to symmetrical tendency of the $S(x)$ function (not shown here).

Fig. 3 shows an influence of the parameter γ_{cs} on an open–circuit (OC) and is organized in the same manner as Fig. 2 with the same annihilation rate constants. A total current density is equal to zero for an open–circuit voltage V_{oc}. Therefore, the currents J_n and J_p presented in part (b) have opposite signs and they are symmetrical about the zero axis. Fig. 3(c) illustrates the electron and hole densities as a function of a distance from electrodes. In contrast to the case of SC, we observe symmetrical curves with respect to the middle of a sample. Such a behavior has been reported in previous steady–state drift–diffusion studies [24]. The increasing of annihilation rate causes a visible drop of both concentrations in the bulk of sample. Part (d) of Fig. 3 demonstrates a distribution of excitons in space. We observe a symmetrical distribution of the $S(x)$ curve which is a consequence of symmetrical behavior of charge

carriers concentrations. Our calculations clearly illustrate that the density S decreases for higher values of γ_{cs} due to more efficient interaction of excitons with electrons and holes in the bulk of sample.

Fig. 4 shows a short–circuit current, an open–circuit voltage, a fill factor and a power conversion efficiency plotted as a function of γ_{cs}. We can see that these parameters are constant for $\gamma_{cs} < 10^{-16}$ m^3 s^{-1}. If γ_{cs} reaches the range 10^{-16}–10^{-15} m^3 s^{-1}, then all photovoltaic parameters start to decrease monotonically. For an open–circuit voltage V_{oc}, an almost linear decreasing (in semi–log plot) is observed. Fig. 4(d) presents that a magnitude of PCE has dropped about a several percent. When we take into account that $\gamma_{cs} = 3 \times 10^{-14}$ m^3 s^{-1} for P3HT (which is usually used in polymer photovoltaics), then the conclusion is that the process of excitons annihilation on charge carriers is not a beneficial phenomenon for polymer solar cells.

3.2 Influence of exciton mobility

It is known that photovoltaic parameters, in particular a fill factor, can significantly depend on values of charge carrier mobilities for organic solar cells [23]. Therefore, we decided to investigate a possible impact of the exciton mobility on J_{sc}, V_{oc}, FF and PCE in the presence of the annihilation process.

Fig. 5 shows numerical results drawn for different exciton mobilities in the case of short–circuit current J_{sc}. Part (a) presents results of the current density plotted as a function of voltage. We can see that increasing of μ_s leads to lower values of J_{sc}. Spatial distributions of the components J_n and J_p are depicted in part (b), while parts (c) and (d) demonstrate spatial distributions

of charge carriers and excitons, respectively. The increasing of exciton mobility causes a slight drop of electrons and holes concentrations observed mainly near electrodes. It correlates with a behavior of $S(x)$ curve. We observe a plateau–like behaviour for lower magnitudes of μ_s and this plateau becomes shorter when the mobility μ_s increases. Obviously, excitons with higher mobility reach electrodes faster than slower excitons where they are quenched (see boundary condition given by Eq. (22)). Therefore, excitons at the electrical contacts cannot participate to the process of dissociation into separated electrons and holes. It leads to lower concentrations of charge carriers near electrodes and also to decreasing of a total electrical current. A slight asymmetrical shape of $S(x)$ curve is a consequence of different mobilities of electrons and holes, similarly to results presented in Fig. 2(d). For the case of V_{oc}, the changes of the densities n, p and S are smaller than for SC conditions (see supplementary material, Fig. S3).

Fig. 6 presents J_{sc}, V_{oc}, FF and PCE plotted as a function of the exciton mobility calculated for different annihilation rate constants. We can clearly see that values of all photovoltaic parameters decrease with higher magnitudes of the rate constants γ_{cs}. The role of the exciton mobility looks as follows. The fill factor is the only parameter which increases with μ_s. However, this tendency is slight and noticeable for higher values of γ_{cs}. It has been recently reported that higher magnitudes of charge carrier mobilities lead to greater values of FF [23,41]. Therefore, we can conclude that mobilities of all particles, including quasi–particles (excitons), cause an increasing of the fill factor. Other photovoltaic parameters decrease monotonically with the mobility μ_s. We can see that when the probability of annihilation process is greater, then this decreasing becomes slight.

3.3 Influence of recombination reduction parameter

The next step is to investigate the contribution of the recombination to the annihilation process. In organic materials, a bimolecular recombination is usually described by the Langevin model [4]. Recently, systematical studies of donor–acceptor bulk heterojunction structures have demonstrated that an experimental recombination coefficient γ_R is lower than the Langevin coefficient γ_L [42–44]. The ratio γ_R/γ_L is called the recombination reduction factor ξ and its magnitude is in the range 10^{-4}–10^{-1}. In this work, we treat ξ as a numerical parameter which lowers the bimolecular recombination.

Fig. 7 shows computational results of current density versus voltage (a), spatial distributions of current density components J_n and J_p (b), concentrations of electrons and holes as a function of a distance from electrodes (c) and a distribution of excitons in space (d). All parts of Fig. 7 are plotted for different recombination reduction factors ξ in the case of an open–circuit voltage V_{oc}. We can see that a decreasing of the parameter ξ leads to higher concentrations of electrons and holes. This is an obvious consequence of a reduced recombination of charge carriers. The concentration of excitons decreases for lower values of ξ. The conclusion is that more electrons and holes can interact with excitons leading to their annihilation. The results obtained for short–circuit current are presented in supplementary material (Fig. S4). In this case, we do not observe visible changes of concentrations n, p and S with the decreasing of parameter ξ.

Fig. 8 shows all photovoltaic parameters presented versus the recombination reduction factor. Calculations were done for different annihilation rate con-

stants. We can see that the short–circuit current, the open–circuit voltage and the power conversion efficiency decrease monotonically with ξ. The observed changes of the J_{sc} are very slight and noticeable when the factor ξ approaches unity. The fill factor behaves differently than other parameters. It starts to increase for small values of ξ and reaches a maximum. The annihilation process lowers the magnitude of FF and shifts the maximum towards larger ξ.

4 Summary

In summary, we have analyzed the process of excitons annihilation on charge carriers. The calculations based on the one–dimensional transient drift–diffusion model have been done. We have studied an influence of the excitons interaction with charge carriers on photovoltaic parameters (the short–circuit current, the open–circuit voltage, the fill factor and the power conversion efficiency). A visible decreasing of the organic photocells efficiency with the annihilation process has been observed for $\gamma_{cs} > 10^{-15}$ m^3 s^{-1}.

5 Acknowledgment

Calculations were carried out at the Academic Computer Centre (CI TASK) in Gdańsk.

6 Appendix A. Supplementary data

Supplementary data (for discretized equations used in Scharfetter–Gummel method, an energy level diagram for fitting procedure, the J–V characteristics calculated for wide range of annihilation rate constants, results for open–circuit with different exciton mobilities and results for short–circuit with different recombination reduction factors) associated with this article can be found, in the online version, at ...

7 Appendix B. Numerical program

Program Title: `drift-diffusion_pv_organic`

Program Files doi: `http://dx.doi.org/10.17632/ssyj7gfrx7.1`

Licensing provisions: MIT

Programming language: C++

References

[1] B.A. Gregg, M.C. Hanna, J. Appl. Phys. 93 (2003) 3605–3614.

[2] B.A. Gregg, J. Phys. Chem. B 107 (2003) 4688–4698.

[3] K.C. Kao, W. Hwang, Electrical Transport in Solids with Particular Reference to Organic Semiconductors, Pergamon Press, Oxford, 1981.

[4] M. Pope, C.E. Swenberg, Electronic Processes in Organic Crystals and Polymers, second ed., Oxford University Press, Oxford, 1999.

[5] J. Kalinowski, W. Stampor, J. Szmytkowski, D. Virgili, M. Cocchi, V. Fattori, C. Sabatini, Phys. Rev. B 74 (2006) 085316.

[6] S. Reineke, K. Walzer, K. Leo, Phys. Rev. B 75 (2007) 125328.

[7] M Shao, L. Yan, M. Li, I. Iliab, B. Hu, J. Mater. Chem. C 1 (2013) 1330–1336.

[8] Q. Wang, I.W.H. Oswald, M.R. Perez, H. Jia, B.E. Gnade, M.A. Omary, Adv. Funct. Mater. 23 (2013) 5420–5428.

[9] D. Yuan, L. Niu, Q. Chen, W. Jia, P. Chen, Z. Xiong, Phys. Chem. Chem. Phys. 17 (2015) 27609–27614.

[10] J.S. Price, N.C. Giebink, Appl. Phys. Lett. 106 (2015) 263302.

[11] H. van Eersel, P.A. Bobbert, R.A.J. Janssen, R. Coehoorn, J. Appl. Phys. 119 (2016) 163102.

[12] A.J. Ferguson, N. Kopidakis, S.E. Shaheen, G. Rumbles, J. Phys. Chem. C 112 (2008) 9865–9871.

[13] I.A. Howard, J.M. Hodgkiss, X. Zhang, K.R. Kirov, H.A. Bronstein, C.K. Williams, R.H. Friend, S. Westenhoff, N.C. Greenham, J. Am. Chem. Soc. 132 (2010) 328–335.

[14] A.J. Ferguson, N. Kopidakis, S.E. Shaheen, G. Rumbles, J. Phys. Chem. C 115 (2011) 23134–23148.

[15] J M. Hodgkiss, S. Albert–Seifried, A. Rao, A.J. Barker, A.R. Campbell, R.A. Marsh, R.H. Friend, Adv. Funct. Mater. 22 (2012) 1567-1577.

[16] J. Szmytkowski, Phys. Status Sol. RRL 6 (2012) 300–302.

[17] J. Szmytkowski, Semicond. Sci. Technol. 28 (2013) 052002.

[18] L. Tzabari, V. Zayats, N. Tessler, J. Appl. Phys. 114 (2013) 154514.

[19] B. Verreet, A. Bhoolokam, A. Brigeman, R. Dhanker, D. Cheyns, P. Heremans, A. Stesmans, N.C. Giebink, B.P. Rand, Phys. Rev. B 90 (2014) 115304.

[20] J. Szmytkowski, Semicond. Sci. Technol. 29 (2014) 075022.

[21] W.A. Koopman, M. Natali, G.P. Donati, M. Muccini, S. Toffanin, ACS Photonics 4 (2017) 282–291.

[22] R. Coehoorn, L. Zhang, P.A. Bobbert, H. van Eersel, Phys. Rev. B 95 (2017) 134202.

[23] W. Tress, Organic Solar Cells: Theory, Experiment, and Device Simulation, Springer, Berlin, 2014.

[24] L.J.A. Koster, E.C.P. Smits, V.D. Mihailetchi, P.W.M. Blom, Phys. Rev. B 72 (2005) 085205.

[25] T. Kirchartz, B.E. Pieters, K. Taretto, U. Rau, J. Appl. Phys. 104 (2008) 094513.

[26] G.A. Buxton, N. Clarke, Modelling Simul. Mater. Sci. Eng. 15 (2007) 13–26.

[27] J.A. Barker, C.M. Ramsdale, N.C. Greenham, Phys. Rev. B 67 (2003) 075205.

[28] I. Hwang, N.C. Greenham, Nanotechnology 19 (2008) 424012.

[29] I. Hwang, C.R. McNeill, N.C. Greenham, J. Appl. Phys. 106 (2009) 094506.

[30] Z.S. Wang, W.E.I. Sha, W.C.H. Choy, J. Appl. Phys. 120 (2016) 213101.

[31] H. Bouchriha, G. Delacote, P. Delannoy, M. Schott, J. Physique 35 (1974) 577–587.

[32] L. Lüer, S. Hoseinkhani, D. Polli, J. Crochet, T. Hertel, G. Lanzani, Nature Phys. 5 (2009) 54–58.

[33] D.P. Hoffman, S.Y. Leblebici, A.M. Schwartzberg, R.A. Mathies, J. Phys. Chem. Lett. 6 (2015) 2919–2923.

[34] L. Onsager, J. Chem. Phys. 2 (1934) 599–615.

[35] C.L. Braun, J. Chem. Phys. 80 (1984) 4157–4161.

[36] T.E. Goliber, J.H. Perlstein, J. Chem. Phys. 80 (1984) 4162–4167.

[37] L. Lu, W. Chen, T. Xu, L. Yu, Nature Comm. 6 (2015) 7327.

[38] V.D. Mihailetchi, L.J.A. Koster, J.C. Hummelen, P.W.M. Blom, Phys. Rev. Lett. 93 (2004) 19–22.

[39] M. Hilczer, M. Tachiya, J. Phys. Chem. C 114 (2010) 6808–6813.

[40] Z. He, C. Zhong, X. Huang, W.Y. Wong, H. Wu, L. Chen, S. Shijian, Y. Cao, Adv. Mater. 23 (2011) 4636–4643.

[41] L.M. Andersson, C. Müller, B.H. Badada, F. Zhang, U. Würfel, O. Inganäs, J. Appl. Phys. 110 (2011) 024509.

[42] A. Pivrikas, N.S. Sariciftci, G. Juška, R. Österbacka, Prog. Photovolt: Res. Appl. 15 (2007) 677–696.

[43] G. Lakhwani, A. Rao, R.H. Friend, Annu. Rev. Phys. Chem. 65 (2014) 557–81.

[44] A. Wagenpfahl, J. Phys.: Condens. Matter 29 (2017) 373001.

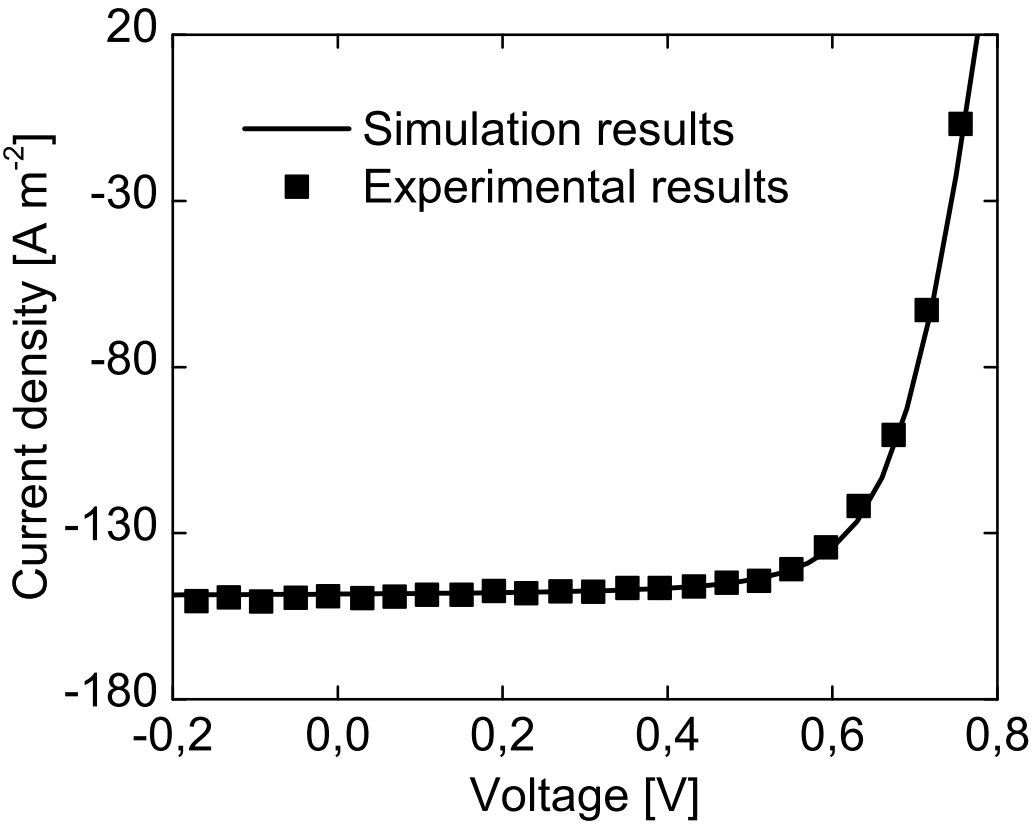

Fig. 1. Numerical (solid line) and experimental (squares) results of current density as a function of voltage for PTB7–Th:$PC_{71}BM$. The experimental points for J–V characteristics are extracted from literature [37]. The parameters used in calculations: $\xi = 5 \times 10^{-2}$, $\mu_s = 1.2 \times 10^{-8}$ m^2 V^{-1} s^{-1}. The process of annihilation is not considered in this fit.

Table 1

The parameters used in simulations and in fitting procedure.

Parameter	Symbol	Numerical value
Length of a photoactive material [37]	L	100 nm
Ion–pair separation distance [30]	a_0	3.5 nm
Effective density of states in conduction band [24,30]	N_c	2.5×10^{25} m^{-3}
Effective density of states in valence band [24,30]	N_v	2.5×10^{25} m^{-3}
Mobility of electrons	μ_n	2.8×10^{-7} m^2 V^{-1} s^{-1}
Mobility of holes	μ_p	5.2×10^{-8} m^2 V^{-1} s^{-1}
Exciton decay rate [40]	k_f	1×10^5 s^{-1}
Schottky barrier height for cathode	ϕ_n	0.15 eV
Schottky barrier height for anode	ϕ_p	0.15 eV
Energy band–gap	E_g	1.22 eV
Relative permittivity [30]	ε_r	3.9
Temperature	T	293 K
Exciton generation rate [37]	G	9.79×10^{27} m^{-3} s^{-1}
Built–in voltage	V_{built}	0.8 V
Spatial grid	Δx	2 nm
Temporal grid	Δt	0.5 ns

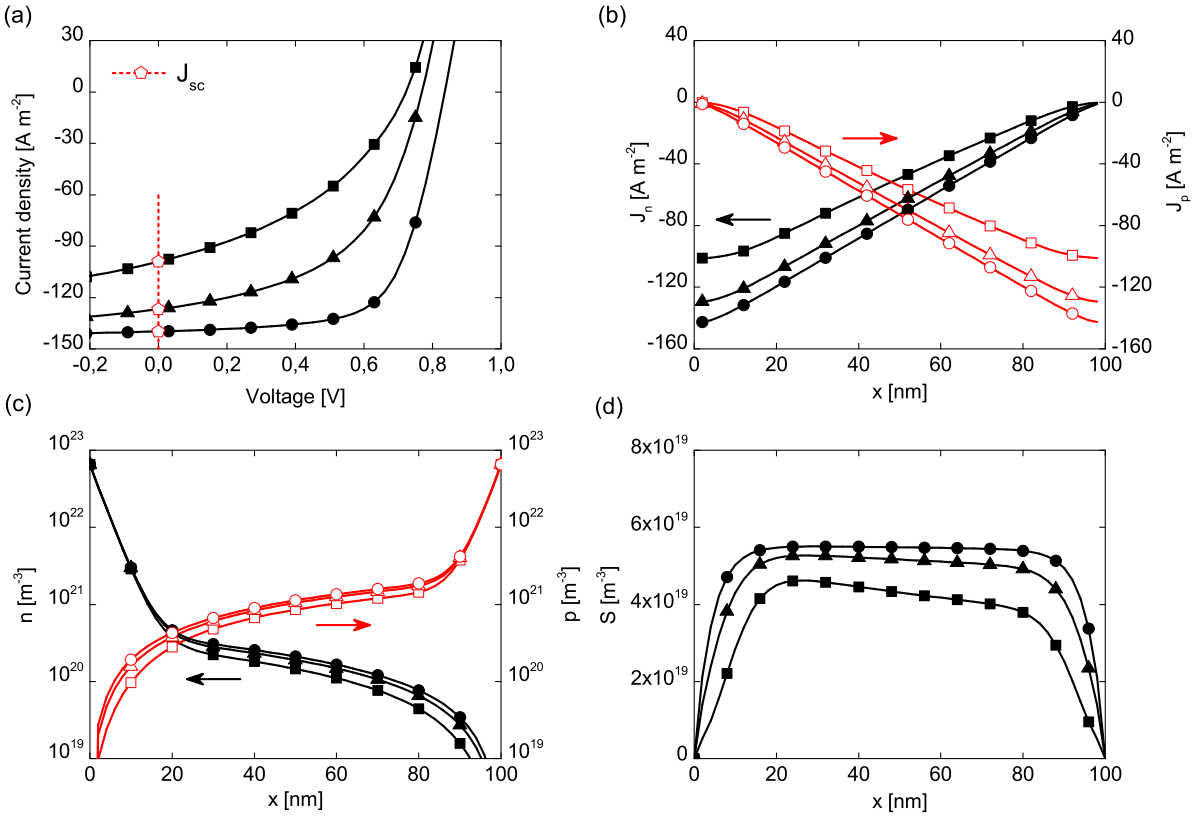

Fig. 2. Numerical results calculated for short–circuit current J_{sc} with different annihilation rate constants. (a) Current density as a function of voltage, (b) current densities for electrons and holes versus distance from cathode, (c) spatial distributions of electrons and holes, (d) a spatial distribution of excitons. Results of simulations are plotted as lines with symbols. Circles, triangles and squares denote the annihilation rate constants ($\gamma_{ns} = \gamma_{ps}$) equal to 10^{-15}, 10^{-14} and 5×10^{-14} m^3 s^{-1}, respectively. Closed and open symbols in parts (b) and (c) are used for electrons and holes, respectively. Parameters used in calculations: $\xi = 10^{-2}$, $\mu_s = 10^{-7}$ m^2 V^{-1} s^{-1}.

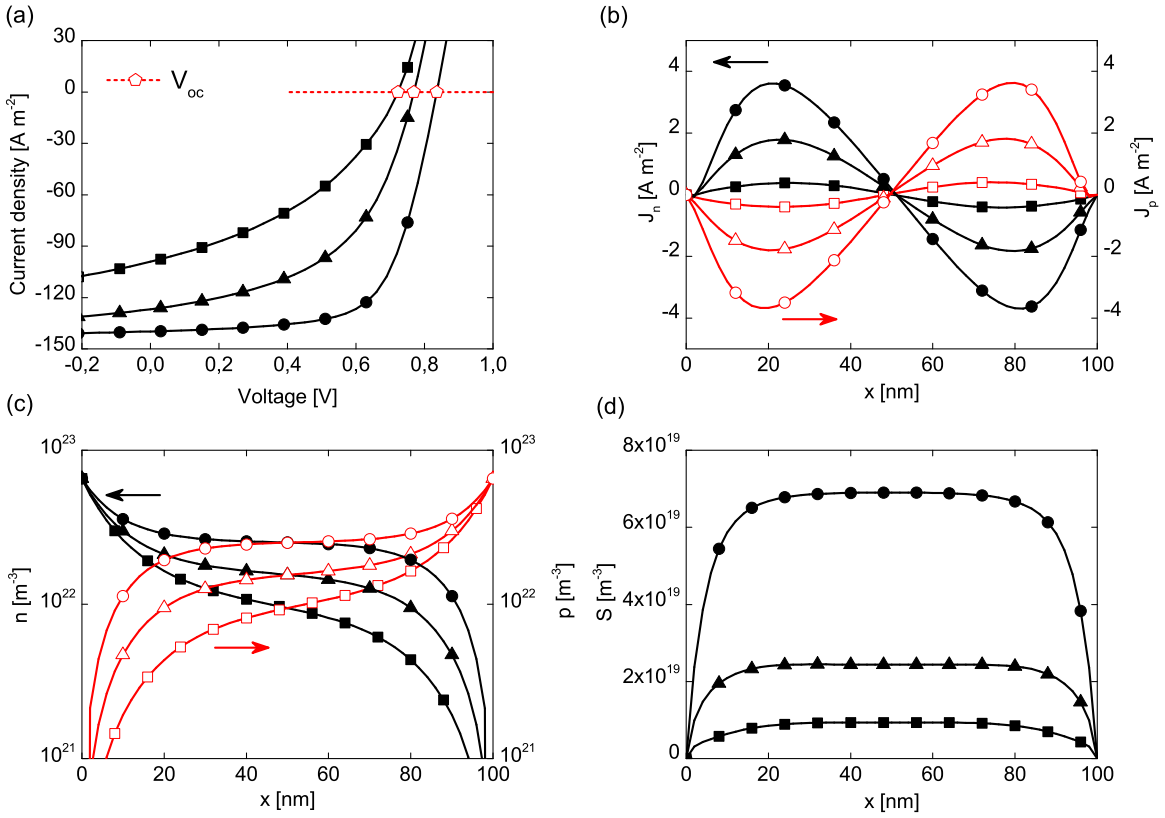

Fig. 3. Numerical results calculated for open–circuit voltage V_{oc} with different annihilation rate constants. (a) Current density as a function of voltage, (b) current densities for electrons and holes versus distance from cathode, (c) spatial distributions of electrons and holes, (d) a spatial distribution of excitons. Results of simulations are plotted as lines with symbols. Circles, triangles and squares denote the annihilation rate constants ($\gamma_{ns} = \gamma_{ps}$) equal to 10^{-15}, 10^{-14} and 5×10^{-14} m^3 s^{-1}, respectively. Closed and open symbols in parts (b) and (c) are used for electrons and holes, respectively. Parameters used in calculations: $\xi = 10^{-2}$, $\mu_s = 10^{-7}$ m^2 V^{-1} s^{-1}.

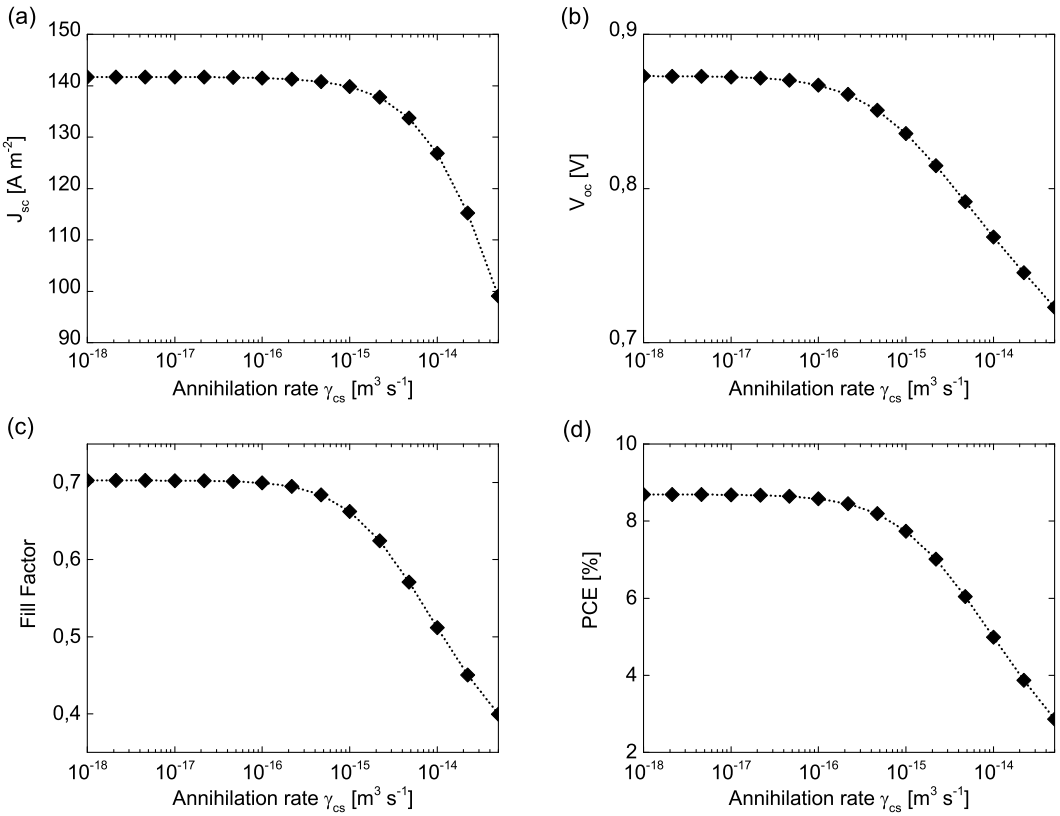

Fig. 4. Short–circuit current (a), open–circuit voltage (b), fill factor (c), and power conversion efficiency (d) as a function of annihilation rate constant ($\gamma_{ns} = \gamma_{ps}$). Symbols present numerical results. Dotted lines are plotted as guides for the eye. Parameters used in calculations: $\xi = 10^{-2}$, $\mu_s = 10^{-7}$ m^2 V^{-1} s^{-1}.

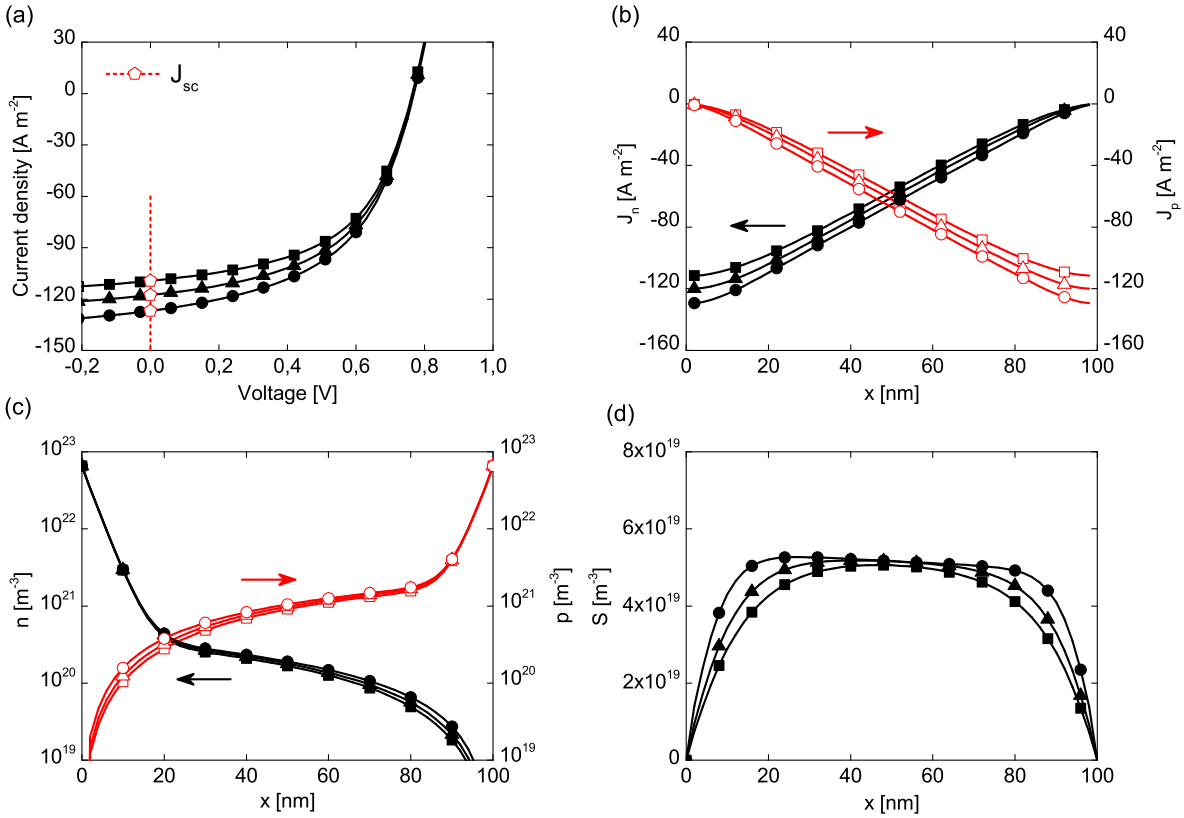

Fig. 5. Numerical results calculated for short–circuit current J_{sc} with different exciton mobilities. (a) Current density as a function of voltage, (b) current densities for electrons and holes versus distance from cathode, (c) spatial distributions of electrons and holes, (d) a spatial distribution of excitons. Results of simulations are plotted as lines with symbols. Circles, triangles and squares denote the exciton mobilities equal to 10^{-7}, 5×10^{-7} and 10^{-6} m^2 V^{-1} s^{-1}, respectively. Closed and open symbols in parts (b) and (c) are used for electrons and holes, respectively. Parameters used in calculations: $\xi = 10^{-2}$, $\gamma_{ns} = \gamma_{ps} = 10^{-14}$ m^3 s^{-1}.

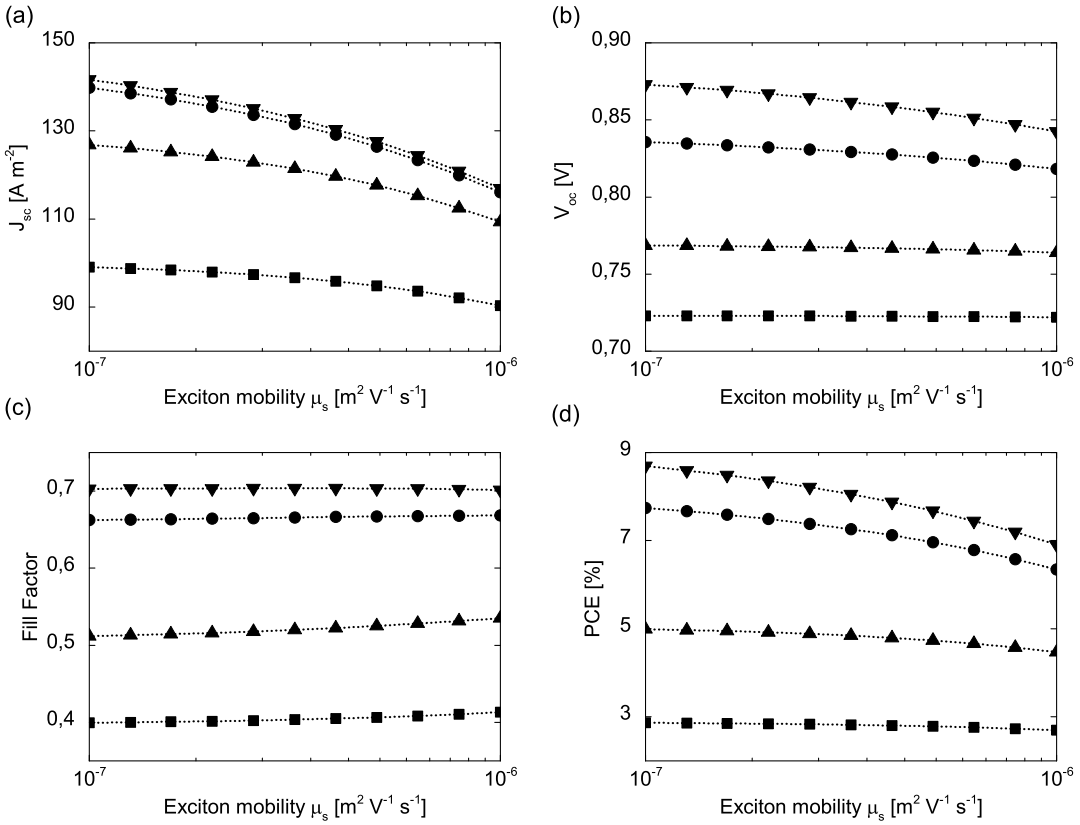

Fig. 6. Short–circuit current (a), open–circuit voltage (b), fill factor (c), and power conversion efficiency (d) as a function of exciton mobility. Symbols present numerical results. Down triangles, circles, triangles and squares denote the annihilation rate constants ($\gamma_{ns} = \gamma_{ps}$) equal to 0, 10^{-15}, 10^{-14} and 5×10^{-14} m^3 s^{-1}, respectively. The recombination reduction factor $\xi = 10^{-2}$. Dotted lines are plotted as guides for the eye.

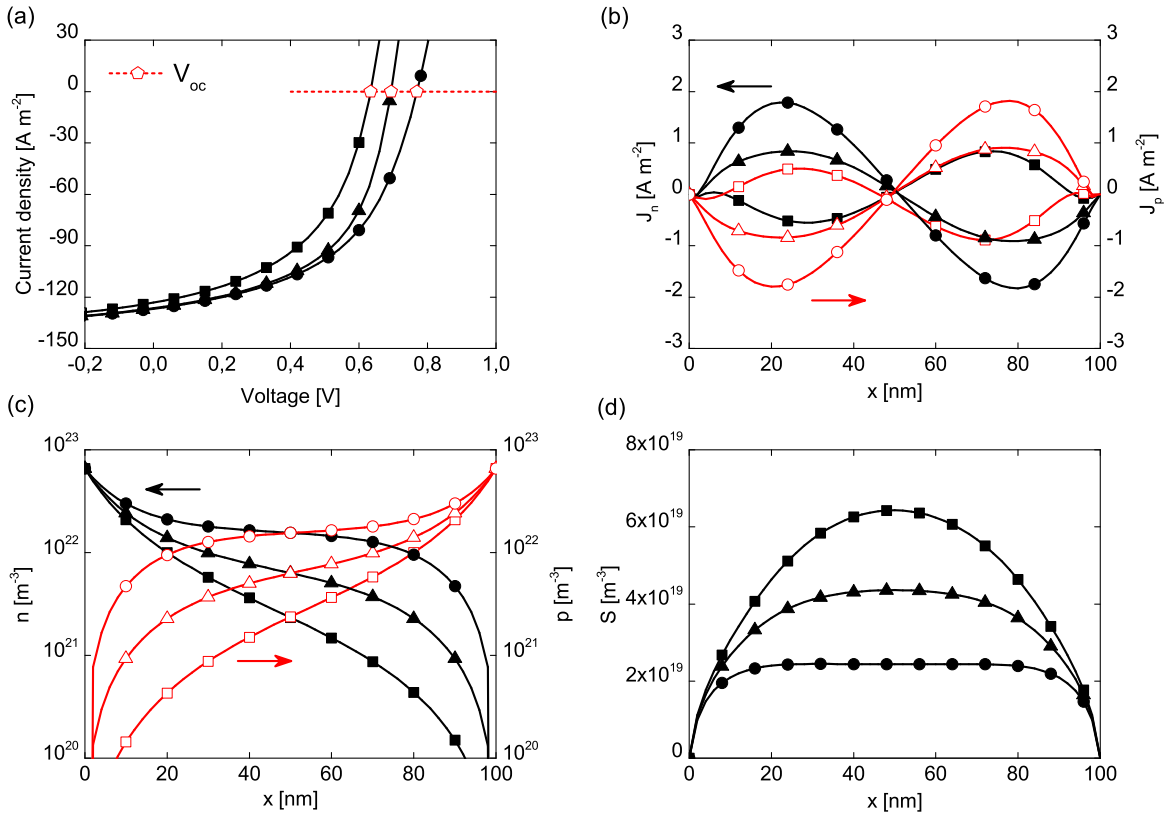

Fig. 7. Numerical results calculated for open–circuit voltage V_{oc} with different recombination reduction factors. (a) Current density as a function of voltage, (b) current densities for electrons and holes versus distance from cathode, (c) spatial distributions of electrons and holes, (d) a spatial distribution of excitons. Results of simulations are plotted as lines with symbols. Circles, triangles and squares denote the recombination reduction factors equal to 10^{-2}, 10^{-1} and 1, respectively. Closed and open symbols in parts (b) and (c) are used for electrons and holes, respectively. Parameters used in calculations: $\gamma_{ns} = \gamma_{ps} = 10^{-14}$ m^3 s^{-1}, $\mu_s = 10^{-7}$ m^2 V^{-1} s^{-1}.

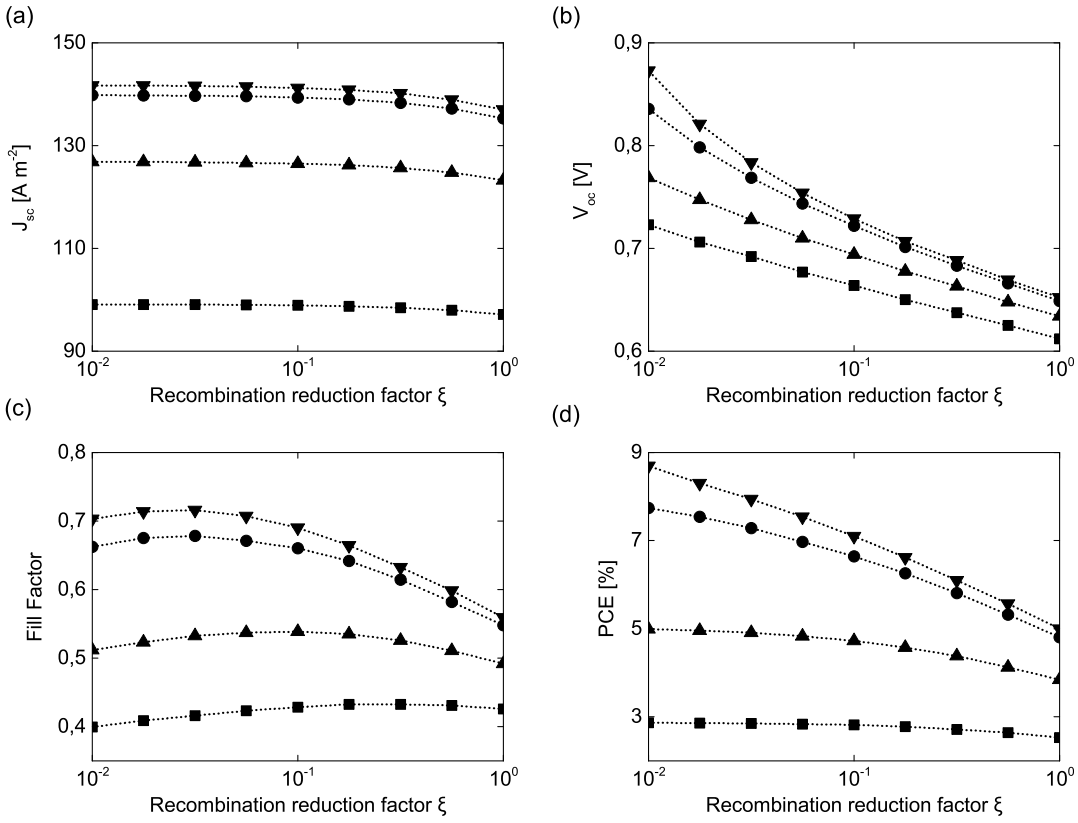

Fig. 8. Short–circuit current (a), open–circuit voltage (b), fill factor (c), and power conversion efficiency (d) as a function of recombination reduction factor. Symbols present numerical results. Down triangles, circles, triangles and squares denote the annihilation rate constants ($\gamma_{ns} = \gamma_{ps}$) equal to 0, 10^{-15}, 10^{-14} and 5×10^{-14} m^3 s^{-1}, respectively. The exciton mobility $\mu_s = 10^{-7}$ m^2 V^{-1} s^{-1}. Dotted lines are plotted as guides for the eye.